

Interstellar Extinction Curve Variations Toward the Inner Milky Way: A Challenge to Observational Cosmology

David M. Nataf^{1,2*}, Oscar A. Gonzalez³, Luca Casagrande^{1,2}, Gail Zasowski^{4,5,2}, Christopher Wegg⁶, Christian Wolf¹, Andrea Kunder⁷, Javier Alonso-Garcia^{8,9}, Dante Minniti^{9,10,11}, Marina Rejkuba^{12,13}, Roberto K. Saito¹⁴, Elena Valenti¹², Manuela Zoccali^{15,9}, Radosław Poleski^{16,17}, Grzegorz Pietrzyński^{16,18}, Jan Skowron¹⁶, Igor Soszyński¹⁶, Michał K. Szymański¹⁶, Andrzej Udalski¹⁶, Krzysztof Ulaczyk^{16,19}, Łukasz Wyrzykowski¹⁶

¹Research School of Astronomy and Astrophysics, Australian National University, Canberra, ACT 2611, Australia

²Kavli Institute for Theoretical Physics, University of California, Santa Barbara, CA 93106

³European Southern Observatory, 19001 Casilla Santiago 19, Chile

⁴NSF Astronomy and Astrophysics Postdoctoral Fellow

⁵Department of Physics & Astronomy, Johns Hopkins University, Baltimore, MD, 21218, USA

⁶Max-Planck-Institut für Extraterrestrische Physik, Giessenbachstrasse, 85748 Garching, Germany

⁷Leibniz-Institut für Astrophysik Potsdam (AIP), An der Sternwarte 16, D-14482 Potsdam, Germany

⁸Unidad de Astronomía, Facultad Cs. Básicas, Universidad de Antofagasta, Avda. U. de Antofagasta 02800, Antofagasta, Chile

⁹Millennium Institute of Astrophysics, Av. Vicuña Mackenna 4680, Macul, Santiago, Chile

¹⁰Vatican Observatory, 00120 Vatican City State, Italy

¹¹Departamento de Ciencias Físicas, Universidad Andres Bello, Republica 220, Santiago, Chile

¹²European Southern Observatory, Karl-Schwarzschild-Strasse 2, 85748 Garching, Germany

¹³Excellence Cluster Universe, Boltzmannstr. 2, 85748, Garching, Germany

¹⁴Departamento de Física-Universidade Federal de Sergipe,

Rod. Marechal Rondon s/n-Jardim Rosa Elze, Sao Cristovao, 49.100-000, Sergipe, Brazil

¹⁵Instituto de Astrofísica, Facultad de Física, Pontificia Universidad Católica de Chile, Av. Vicuña Mackenna, Santiago, Chile

¹⁶Warsaw University Observatory, Al. Ujazdowskie 4, 00-478 Warszawa, Poland

¹⁷Department of Astronomy, Ohio State University, 140 W. 18th Ave., Columbus, OH 43210

¹⁸Universidad de Concepción, Departamento de Astronomía, Casilla 160-C, Concepción, Chile

¹⁹Department of Physics, University of Warwick, Gibbet Hill Road, Coventry, CV4 7AL, UK

Accepted Received ; in original form.....

ABSTRACT

We investigate interstellar extinction curve variations toward $\sim 4^\circ$ of the inner Milky Way in $VIJK_s$ photometry from the OGLE-III and VVV surveys, with supporting evidence from diffuse interstellar bands and $F435W$, $F625W$ photometry. We obtain independent measurements toward $\sim 2,000$ sightlines of A_I , $E(V-I)$, $E(I-J)$, and $E(J-K_s)$, with median precision and accuracy of 2%. We find that the variations in the extinction ratios $A_I/E(V-I)$, $E(I-J)/E(V-I)$ and $E(J-K_s)/E(V-I)$ are large (exceeding 20%), significant, and positively correlated, as expected. However, both the mean values and the trends in these extinction ratios are drastically shifted from the predictions of Cardelli and Fitzpatrick, *regardless of how R_V is varied*. Furthermore, we demonstrate that variations in the shape of the extinction curve has at least two degrees of freedom, and not one (e.g. R_V), which we conform with a principal component analysis. We derive a median value of $\langle A_V/A_{K_s} \rangle = 13.44$, which is $\sim 60\%$ higher than the “standard” value. We show that the *Wesenheit* magnitude $W_I = I - 1.61(I - J)$ is relatively impervious to extinction curve variations.

Given that these extinction curves are linchpins of observational cosmology, and that it is generally assumed that R_V variations correctly capture variations in the extinction curve, we argue that systematic errors in the distance ladder from studies of type Ia supernovae and Cepheids may have been underestimated. Moreover, the reddening maps from the *Planck* experiment are shown to systematically overestimate dust extinction by $\sim 100\%$, and lack sensitivity to extinction curve variations.

Key words: ISM: dust, extinction – ISM: lines and bands

* Email: david.nataf@anu.edu.au

1 INTRODUCTION

1.1 Interstellar extinction curve towards the inner Milky Way

The interstellar extinction curve toward the inner Milky Way has long been argued to be “non-standard”. This was first suggested from observations of planetary nebulae. Stasińska et al. (1992) analyzed data on the Balmer decrement and the ratio of radio to $H\beta$, and argued for an extinction curve that declines more rapidly with increasing wavelength (i.e. steeper) than the $R_V = A_V/E(B - V) = 3.1$ extinction curve, either $R_V = 2.0$ or $R_V = 2.7$ depending on the choice of parameterization, a conclusion supported by Tylenda et al. (1992) using a similar method. Pottasch & Zijlstra (1994) confirm a systematic difference in extinction derived from the radio/ $H\beta$ flux ratio and the Balmer decrement using additional measurements. Ruffle et al. (2004) obtain additional measurements for a set of lines ([OIII], $H\alpha$, etc) and estimate a mean extinction curve toward the inner Galaxy of $\langle R_V \rangle = 2.0$.

Separately, and independently, the anomalous dereddened colours of standard crayons in and near the Galactic bulge such as RR Lyrae stars have also suggested a non-standard extinction curve (Stutz et al. 1999). The evidence has since accumulated from measurements of magnitude-colour slope of red clump (RC) centroids in optical photometry (Udalski 2003b; Nataf et al. 2013b, following the work of Stanek 1996 and Wozniak & Stanek 1996) from the *Optical Gravitational Lensing Experiment* (OGLE), in optical *Hubble Space Telescope* (HST) photometry (Revniytsev et al. 2010), in ground-based near-infrared (IR) photometry (Nishiyama et al. 2009), with a combination of ground-based near-IR and space-based mid-IR photometry from the *Spitzer Space Telescope* (Zasowski et al. 2009), in optical photometry of RR Lyrae stars (Pietrukowicz et al. 2012, 2015), with photometry of individual red giant stars in near-IR photometry (Gosling et al. 2009), and from line-emission ratios toward the Galactic centre (Fritz et al. 2011). For dissenting analyses, see Kunder et al. (2008) and Pottasch & Bernard-Salas (2013).

The mean shape and variation of the extinction curve toward the bulge is of concern to the fields of microlensing (e.g. Bachelet et al. 2012; Henderson et al. 2014; Yee et al. 2015), extremely-metal-poor stars (Howes et al. 2014, 2015), Galactic globular clusters (Massari et al. 2012; Saracino et al. 2015), and Galactic structure (Cao et al. 2013; Wegg et al. 2015), among others. Minniti et al. (2014) argued that a large fraction of the interstellar dust toward the bulge is located in a single “great dark lane”. The level of interest and controversy has thus been amply justified and driven by the research needs.

Nataf et al. (2013b) followed up on the issue of extinction curve variations by combining measurements of the optical reddening $E(V - I)$ from ~ 100 deg² of photometry from OGLE-III with the corresponding measurements of the near-IR reddening $E(J - K_s)$ from the *VISTA Variables in the Via Lactea* (VVV) survey (Gonzalez et al. 2012). The mean extinction ratios measured were $A_I/E(V - I) \approx 1.22$, and $E(J - K_s)/E(V - I) \approx 0.34$, both with statistically significant $1-\sigma$ scatter of $\sim 10\%$, and both approximately consistent in the mean with the $R_V = 2.5$ interstellar extinction curve from Cardelli et al. (1989), but not consistent with the mean

value of $A_I/E(V - I) = 1.44$ measured toward the Large Magellanic Cloud (LMC) (Udalski 2003b). One of the results from Nataf et al. (2013b), that the optical extinction could be parameterized as $A_I = 0.7465E(V - I) + 1.3700E(J - K_s)$, has since been confirmed by Pietrukowicz et al. (2015) and also used by Kunder et al. (2015), in their studies of bulge RR Lyrae stars.

A legitimate concern that one can level against the findings of Nataf et al. (2013b) is that the argument is dependent on assuming that the “standard” extinction curve is that of Cardelli et al. (1989). In contrast, both Fitzpatrick (1999) and Fitzpatrick & Massa (2007) find substantially steeper mean Galactic extinction curves for $\lambda \gtrsim 6000$ Å even if one fixes $R_V \approx 3.1$. Indeed, the conclusion of Kunder et al. (2008) that the interstellar extinction toward the bulge is standard, uses the curve of Fitzpatrick (1999) to anchor what “standard” means – if Kunder et al. (2008) had relied upon the analysis of Cardelli et al. (1989) their conclusion would have been reversed. Schlafly & Finkbeiner (2011) have recently demonstrated that $R_V = 3.1$ curve from Fitzpatrick (1999) yields a much better fit to optical photometry of main-sequence turnoff stars in the northern Galactic halo than that of Cardelli et al. (1989), a conclusion that Wolf (2014) confirmed using quasi-stellar objects (QSOs) as standard crayons. Babusiaux et al. (2014) recently derived arguably self-consistent distances to Galactic bulge stars by assuming the extinction curve of Fitzpatrick & Massa (2007).

This continuing discrepancy is thus inevitable due to the large number of degrees of freedom. When one can vary not just the parameter R_V but also the choice of parameterization (Cardelli et al. 1989, Fitzpatrick 1999, etc), one has a lot of flexibility with which to fit extinction data. A compelling option with which to resolve this discrepancy is to acquire more photometry and thus more colours, and that is what we do in this investigation. Similarly to Nataf et al. (2013b), our combination of OGLE-III and VVV photometry allows us to measure $A_I/E(V - I)$ and $E(J - K_s)/E(V - I)$. What we also do, by matching sources between the two catalogues, is measure the reddening ratio $E(I - J)/E(V - I)$, for which the different parameterizations and different values of R_V yield specific and distinct predictions.

The structure of this paper is as follows. In Section 1.2 we discuss the relevance of the inner Milky Way extinction curve to cosmology. In Section 2 we describe the raw data used in this investigation. We explain our methodology in Section 3, the expectations from theory are stated in Section 4, present our results in Section 5, we compare our results to select other investigations in Section 6, and our conclusions in Section 7.

1.2 Extinction towards Type Ia Supernovae and Extragalactic Cepheids

Nataf et al. (2013b) argued that there may be a link between the extinction curve variations observed toward the inner Milky Way and observations of SN Ia, toward which low values of R_V are common (e.g. Chotard et al. 2011; Goobar et al. 2014). The Carnegie Supernovae Project (Burns et al. 2014) has measured densely-sampled light curves in 8-10 bandpasses covering the optical and near-IR

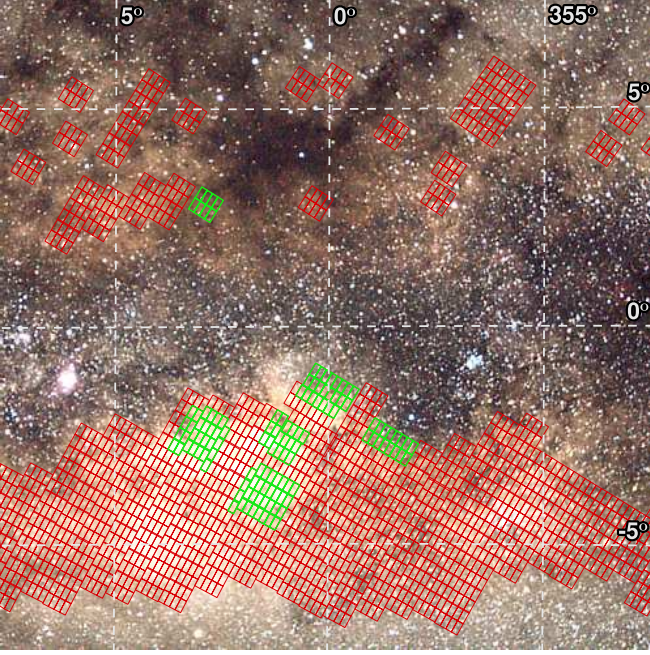


Figure 1. Subset of OGLE-III subfields shown in red overlaid on an optical image of the Galactic bulge with Galactic coordinate system shown as well. The subfields used in this work, for which we also use the matching VVV photometry, are shown in green.

wavelength regime, and confirm steeper-than-standard extinction curves as common – they report a mean $R_V = 2.15 \pm 0.16$ toward their sample. Similarly, Rigault et al. (2015) find that the distance dispersion toward type Ia SNe is minimised if they assume $R_V = 1.7$ as the mean of their sample, though Jones et al. (2015) have demonstrated that this result may emerge from the assumption that star-forming and quiescent galaxies have identical interstellar extinction curves.

Phillips et al. (2013) has shown that this extinction is likely interstellar rather than circumstellar extinction, as the ratio of the equivalent width of the diffuse interstellar band at 5780 Å to the inferred extinction in V -band is consistent with the value for the Milky Way interstellar medium (ISM). Burns et al. (2014) found that many of the type Ia SNe with low values of R_V are also high-velocity events. In turn, Wang et al. (2013) argue that high-velocity type Ia SNe are substantially more concentrated in the inner and brighter regions of host galaxies. Thus, the findings of a steeper extinction curve toward the inner Milky Way (also recently demonstrated for the Andromeda galaxy, see Dong et al. 2014) may be consistent what is found from type Ia SNe host galaxies.

These findings continue to be controversial, as the R_V values seemingly ubiquitous toward type Ia SNe are believed to be rare in the Milky Way, and some have argued that they emerge due to a degeneracy between extinction curve variations and intrinsic colour variations of type Ia SNe (Scolnic et al. 2014). As manifestly plausible as the argument of colour variations clearly is, we suggest that some of the discrepancy is due to the following two reasons:

(i) There is a greater range of extinction curve variations within the Milky Way than commonly believed. In particular, $R_V = 3.1$ may simply be the most common value for the solar neighbourhood, rather than the sharply-peaked mode for the diffuse interstellar medium throughout the Galaxy.

(ii) The widely-used parametric fits of Cardelli et al. (1989) and Fitzpatrick (1999), may simply be incorrect descriptions of nature at the 10% level or greater. In an era of $\lesssim 3\%$ cosmology, this matters, and the systematic error is manifesting as spurious values of R_V .

The anonymous referee notes that the investigation of Fitzpatrick & Massa (2007) already addressed some of these issues. We quote directly from the referee:

“Fitzpatrick & Massa (2007) have demonstrated that interstellar extinction is, in general, far more complex than implied by the CCM [re: Cardelli et al. 1989] relations and that the apparent CCM relations are largely the result of correlated errors. Even CCM never intended the relationships to be considered a “law”, but rather a means to account for a large component of the observed variation. Further, Fitzpatrick & Massa (2009) have shown that optical-NIR extinction curves in the local ISM require at least 2 parameters to explain the observed variations.” - The anonymous referee.

Uncertainties in the mean value of the interstellar extinction curve are also emerging as an issue in the determination of the Cepheid distance scale, which anchors Hubble’s constant H_0 . Altavilla et al. (2004) estimate $R_V = 2.5$ as the best-fit extinction curve parameter toward an archival sample of extragalactic Cepheid light curves. Fausnaugh et al. (2015) used $BVRI$ photometry of Cepheids in the maser-host galaxy NGC 4258, and found that $R_V = 4.9$ provided the best-fit. Nataf (2015) recently showed that the extinction toward the Cepheids in M101 (the Pinwheel galaxy) was better characterised by $A_I/E(V-I) \approx 1.15$ rather than the canonical value of $A_I/E(V-I) \approx 1.47$ (Cardelli et al. 1989). The situation is such that Riess et al. (2011, 2012) have shifted to using H -band observations of Cepheids to infer distances, for which the extinction is believed to be a smaller uncertainty. However, this comes at the cost of a broader PSF (since HST photometry is nearly diffraction-limited) and thus greater blending in H -band, in addition to greater relative flux contributions from colder red giant branch and asymptotic giant branch stars.

In light of these factors we consider plausible the idea that better characterisation of the extinction curve toward the inner Milky Way – an independently interesting and tractable scientific endeavour – may facilitate superior understanding of the extinction toward both Cepheids and type Ia SNe. Though the inner Milky Way may be dismissed as less than 2% of the sky in surface area, it represents no less than $\sim 25\%$ of the stellar mass of the Milky Way (Dwek et al. 1995; Nataf et al. 2013b; Portail et al. 2015), a number which accounts for the bulge alone and does not include the inner disk in which this dust is likely located. Indeed, from Bovy & Rix (2013), we can estimate that the Milky Way’s disk contains three times as much stellar mass in the Galactocentric range $4 \leq R_{GC} \leq 8$ as it does in the outer disk $8 \leq R_{GC} \leq 20$. Thus, the dust extinction we study in this work may be that which characterizes how the Milky Way would appear to outside observers, much more so than the dust extinction curve of the solar neighbourhood, and is thus pertinent to better interpreting extragalactic stel-

lar populations. We note of a recent pre-print posted on astro-ph, which measured a mean extinction curve parameter $R_V = 2.4$ toward a sample of 16 intermediate-redshift quasars.

We are aware of uncertainties in the 3D distribution of dust. Neckel et al. (1980) report $2.6 \leq A_V \leq 3.3$ toward the bulk of our sightlines within 1 Kpc of the Sun, which would contribute most of the extinction measured in our work and thus contradict the statement above concerning the Galactic distribution of dust. On the other hand, Schultheis et al. (2014) find an extinction excess toward the Galactic center located ~ 6 Kpc from the Sun, which Minniti et al. (2014) interprets as a “Great Dark Lane” for the Milky Way. Regardless of the details of how the dust is distributed, we expect the integrated sum of extinction to span a range of Galactocentric radii.

2 DATA

OGLE-III, the third phase of the Optical Gravitational Lensing Experiment, produced photometric maps of the Galactic bulge, parts of the Galactic disk, and the Magellanic Clouds. Observations were taken with the 1.3 meter Warsaw Telescope, located at the Las Campanas Observatory. The camera had eight 2048×4096 detectors, with a scale of approximately $0.26''/\text{pixel}$ yielding a combined field of view $0.6^\circ \times 0.6^\circ$. More detailed descriptions of the instrumentation, photometric reductions and astrometric calibrations are available in Udalski (2003a), Udalski et al. (2008) and Szymański et al. (2011). The photometry is in the *VI* optical filters as calibrated by Landolt standard stars (Landolt 1992). OGLE-III photometry and reddening maps are available for download from the OGLE webpage¹. The fourth phase of the OGLE project (OGLE-IV, Udalski et al. 2015) has actually been underway since 2010, with photometric coverage of about 2,100 square degrees of the Galactic bulge and disk. However, we use OGLE-III photometry in this study for consistency with prior investigations.

The *VISTA Variables in the Via Lactea* (VVV) ESO public survey (Minniti et al. 2010) is a near-IR photometric survey covering 560 deg^2 of the Galactic bulge and southern disk. Observations were carried with the VISTA InfraRed Camera (VIRCAM, Dalton et al. 2006; Emerson & Sutherland 2010), mounted at the 4.1 m telescope VISTA (Visible and Infrared Survey Telescope for Astronomy) telescope (Sutherland et al. 2015), located in its own peak at the ESO Cerro Paranal Observatory in Chile. VIRCAM has a mosaic of 16 Raytheon VIRGO 2048×2048 -pixel detectors, with a scale of $0.339''/\text{pixel}$. VVV observations use the stack of two slightly dithered images to produce a stacked image known as a “Pawprint”. A sequence of 6 offset “Pawprints” is used to cover the gaps between the detectors to produce a full, nearly uniform sky coverage of 1.50 deg^2 known as a “tile”. Images are reduced, astrometrized, and stacked at the Cambridge Astronomy Survey Unit (CASU) using the VISTA Data Flow System pipeline (Emerson et al. 2004; Hambly et al. 2004; Irwin et al. 2004).

VVV photometric catalogues at the “tile” level are also produced at CASU. A detailed description of these VVV catalogues can be found in Saito et al. (2012). For this work we use catalogues obtained using PSF photometry based on DoPHOT (Schechter et al. 1993; Alonso-García et al. 2012) measurements from pawprint stacked *J* and *K_s* band images. CASU photometric catalogues are then used to calibrate the PSF photometry. Final magnitudes are therefore based on the VISTA photometric system. Details on the construction of VVV PSF catalogues can be found in (Alonso-García et al. 2015). Infrared $E(J - K_s)$ reddening maps measured with VVV photometry can be found on the online BEAM calculator².

We use observations from a subset of OGLE-III fields that were selected such that our study would span the range of reddening curve parameters $E(J - K_s)/E(V - I)$ toward the bulge, as measured by Nataf et al. (2013b). The photometric coverage used in this work is shown in Figure 1. For those sightlines, we match to sources identified in VVV photometry, producing a combined *VIJK_s* catalogue, where we leave the near-IR photometry in the original VISTA filter system and do not transform to 2MASS (Skrutskie et al. 2006). The total photometry is then broken up into nearly non-overlapping (and thus independent) rectangles, there is a small amount of overlap when different OGLE-III fields lie slightly atop one another. The rectangles into which the OGLE-III subfields are broken up into are chosen such that the number of RC stars, N_{RC} within the region fit is $100 \leq N_{RC} \leq 200$. The typical angular size of these sightlines is $3' \times 3'$.

3 METHODOLOGY

3.1 Photometric Zero Points of the Red Clump

The mean intrinsic (dereddened) colour of the Galactic bulge RC is measured (Bensby et al. 2013) to be:

$$(V - I)_{RC,0} = 1.06. \quad (1)$$

That is the value adopted by our investigation as the zero-point, it is derived by equating the photometric colours of the main-sequence turnoff and subgiant branch stars studied by Bensby et al. (2013) with their spectroscopic temperatures, as derived from high signal-to-noise, high-resolution spectra. This derivation is consistent with several other determinations:

- The prediction from the BaSTI isochrones (Pietrinferni et al. 2004; Cordier et al. 2007) for a 12 Gyr old, $[\text{Fe}/\text{H}] = 0$ stellar population is $(V - I)_{RC,0} = 1.06$ (Nataf et al. 2014, Table 1);
- Based on empirically-calibrated population parameters (Thompson et al. 2010; Brogaard et al. 2011, 2012; Bragaglia et al. 2014; Cunha et al. 2015) and observed photometry (Sarajedini et al. 2007; Stetson et al. 2003) from 47 Tuc and NGC 6791, and assuming Baade’s window metallicity-distribution function (MDF) (Hill et al. 2011), the Galactic Bulge RC value is $(V - I)_{RC,0} \approx 1.07$. This is marginally lower than that estimated by Nataf et al. (2013b)

¹ <http://ogle.astrouw.edu.pl/>

² <http://mill.astro.puc.cl/BEAM/calculator.php>

using the same method due to the increased best-fit metallicity for NGC 6791.

- The Galactic bulge RC is 0.55 mag redder than Galactic bulge ab-type RR Lyrae (Nataf et al. 2013b), where throughout this discussion we only refer to ab-type RR Lyrae. The Fourier coefficients of the RR lightcurves yield a mean intrinsic RR Lyrae colour of $(V - I)_{RR} = 0.49$ (Pietrukowicz et al. 2015), for an estimated mean intrinsic RC colour of $(V - I)_{RC,0} = 1.04$. Alternatively, we have selected 2,301 RR Lyrae from OGLE-III with four or more V -band observations near minimum light (phase $0.50 \leq \phi \leq 0.78$), and contrasted them to the nearest RC reddening measured by (Nataf et al. 2013b). We kept the data points where the reddening agreed to be better than 0.20 mag in $E(V - I)$ to remove spurious outliers, and for which $(V - I)_{RC} \leq 3.30$, leaving 1,987 RR Lyrae. We find that the ratio of reddening agrees to better than 1% in the mean, and that the difference in reddening is 0.02 mag when we regress the offset to $E(V - I)_{RC} = 0$ – exactly equivalent to the above inferred value of $(V - I)_{RC,0} = 1.04$;

- The near-IR colour $(J - K_s)_{RC,0} = 0.68$ was derived by Gonzalez et al. (2011), based on a determination of $E(B - V) = 0.55$ toward Baade’s window by Zoccali et al. (2008). Applying the conversions from Table 1, which is explained below, this corresponds to $(V - I)_{RC,0} \approx 1.07$;

- The reddening measurements of Gonzalez et al. (2011) were in turn tested by comparing spectroscopic temperatures and photometric temperatures (Rojas-Arriagada et al. 2014). The discrepancy in the zero-point is measured to be no greater than $\Delta E(J - K_s) = -0.006 \pm 0.026$ – consistent with zero;

Our assumed mean colour $(V - I)_{RC,0} = 1.06 \pm 0.03$ is thus well-supported by a diverse array of inferential methods, where the 0.03 mag is a conservative estimate of the 1- σ error from the arguments presented above. A possible concern is that the effect of metallicity variations can be significant: interpolating between the BaSTI-predicted values for $[\text{Fe}/\text{H}] = -0.35$ and $[\text{Fe}/\text{H}] = +0.40$ yields a derivative of $d(V - I)_{RC}/d[\text{Fe}/\text{H}] \approx 0.29 \text{ mag dex}^{-1}$ (Nataf et al. 2014, Table 1), with the effect of variations in age or $[\alpha/\text{Fe}]$ being negligible. However, the total range in the mean metallicity across our fields are no greater than $\sim 0.10 \text{ dex}$ (Gonzalez et al. 2013, see also Rich et al. 2012) and thus the effect is negligible. This emerges due to our choice of sightlines, which are relatively similar in direction, do not span the whole bulge, and thus do not probe a significant spread in mean metallicity.

We use model atmospheres to estimate the intrinsic colours of the bulge RC in the full range of filters used in this work, as well as others that may be of interest to future studies, which we show in Table 1. The atmospheric parameters $\log g = 2.2$ and $[\text{Fe}/\text{H}] = 0$ are typical of the RC (Ness et al. 2013), and $T_{\text{eff}} = 4650\text{K}$ is chosen to agree with the intrinsic colour $(V - I)_{RC,0} = 1.06$. The remaining synthetic colours were computed interpolating over a grid of MARCS model atmosphere (Gustafsson et al. 2008) at the T_{eff} , $\log g$ and $[\text{Fe}/\text{H}]$ quoted above, and appropriate filter transmission curves (see details in Casagrande & VandenBerg 2014). Synthetic optical and 2MASS JHK magnitudes were

transformed into the VISTA system³. The remaining colours emerge from a detailed model atmosphere calculation. Optical colours were computed directly. We also provide the colour determinations for a star with atmospheric parameters $\log g = 2.2$, $[\text{Fe}/\text{H}] = -0.30$, $[\alpha/\text{Fe}] = +0.10$, and $T_{\text{eff}} = 4800\text{K}$. These two model atmospheres together define the vector over which metallicity gradients (and thus temperature gradients, since the colour of the RC is predominantly a function of metallicity) would matter if a study such as this one was extended over a larger swath of the bulge.

For the dereddened apparent magnitude of the RC, we use the equation:

$$I_{RC,0} = 14.3955 - 0.0239 * l + 0.0122 * |b|, \quad (2)$$

where the zero-point is taken from Nataf et al. (2013b), and the derivatives are derived by fitting to the data of Wegg & Gerhard (2013) within the coordinate range $-2.00^\circ \leq l \leq 4.0^\circ$, $|b| \leq 4.5^\circ$. The gradients emerge due to projection effects, as stars toward the Galactic bulge are distributed as a bar. The standard deviation between the fit and the data is 0.018 mag. We have verified that there is no significant evidence for cross-terms or higher-order terms in longitude or latitude for the apparent magnitude. Our zero-point assumption of the apparent magnitude of the RC is, as per the work of Cao et al. (2013), equivalent to assuming:

$$M_{I,RC} = -0.12 - 5 \log(R_0/8.13), \quad (3)$$

where $R_0 = R_{GC,\odot}$ is the distance between the Sun and the Galactic centre. Equation 3 is consistent with the canonical Galactocentric distance of $8.33 \pm 0.11 \text{ Kpc}$ (Chatzopoulos et al. 2015) if $M_{I,RC} = -0.17 \pm 0.03$. From these arguments, the zero-point systematic error (bias) in our extinctions is exactly 0 if $M_{I,RC} = -0.17$ and $R_0 = 8.33$. However, Nataf et al. (2013a) estimated $M_{I,RC} = -0.12$ by means of an empirical calibration, and Stanek & Garnavich (1998) measured $M_{I,RC} = -0.23$ for the solar neighbourhood RC. We thus assume a 1- σ systematic error of 0.05 mag in the values of A_I .

3.2 The Measurement Errors in the Reddening and Extinction

From the arguments in the preceding section, the zero-point (systematic) errors in A_I , $E(V - I)$, $E(I - J)$ and $E(J - K_s)$ are no greater than 0.05 mag, 0.03 mag, 0.03 mag, and 0.02 mag respectively, where the errors on $E(I - J)$ and $E(J - K_s)$ are derived from the error in $E(V - I)$ and the vectors defined by Table 1. These are errors which will shift the entire scale, with the errors in $E(V - I)$, $E(I - J)$ and $E(J - K_s)$ being positively correlated. The total colour error due to mean metallicity variations in our sample goes as $\sim 1/\sqrt{12} \times$ the spread due to metallicity if we use the uniform distribution as a probabilistic proxy, and thus the error from metallicity variations is 0.006 mag, 0.006 mag, 0.005 mag, and 0.007 mag respectively. The systematic errors in the colours are positively-correlated with each other, and negatively correlated with the error in the brightness, since the RC becomes redder and dimmer with increasing metallicity.

³ see <http://casu.ast.cam.ac.uk/surveys-projects/vista/technical/photometry/> for more information on the VISTA photometric system.

The statistical errors in the fit, due to the finite number of RC stars per sightline, average 0.038 mag in A_I , and 0.011 mag in $E(V - I)$. The corresponding errors in $E(I - J)$ and $E(J - K_s)$ are likely smaller than and positively correlated with the error in $E(V - I)$, since both the reddening and the dispersion due to temperature are smaller at these longer wavelengths. The correlation in the statistical error with A_I is virtually zero, as the red giant branch is nearly vertical in the VI colour-magnitude diagram (CMD) at the location of the RC.

These errors are small relative to both the mean values and sample dispersions of $A_I = 1.91 \pm 0.67$, $E(V - I) = 1.61 \pm 0.60$, $E(I - J) = 1.18 \pm 0.40$ and $E(J - K_s) = 0.47 \pm 0.17$ in our sample, where the measured sample means and sample dispersions are discussed in Section 5. We thus measure highly significant extinction and reddening values, with mean accuracies no worse than 3%, 2%, 3%, and 4% respectively, and mean precisions no worse than 2%, 1%, 1%, and 2% respectively. Given that the errors in our reddening values are positively-correlated with one another, the errors in the fractions $E(I - J)/E(V - I)$ and $E(J - K_s)/E(V - I)$ will be even smaller than the errors in the constituent parts.

3.3 Fitting for the Red Clump Magnitude and Colours

The iterative fit for the RC apparent magnitude assumes the same luminosity function as used by [Nataf et al. \(2013b\)](#):

$$N(I)dI = A \exp \left[B(I - I_{RC}) \right] + \frac{N_{RC}}{\sqrt{2\pi}\sigma_{RC}} \exp \left[-\frac{(I - I_{RC})^2}{2\sigma_{RC}^2} \right] + \frac{N_{RBB}}{\sqrt{2\pi}\sigma_{RBB}} \exp \left[-\frac{(I - I_{RBB})^2}{2\sigma_{RBB}^2} \right] + \frac{N_{AGBB}}{\sqrt{2\pi}\sigma_{AGBB}} \exp \left[-\frac{(I - I_{AGBB})^2}{2\sigma_{AGBB}^2} \right]. \quad (4)$$

Further discussion and details on the issues pertaining to this fit, such as how to account for the red giant branch bump (RBB) and asymptotic giant branch bump (AGBB), are by now well-documented in the literature ([Nataf et al. 2011, 2014, 2015](#); [Clarkson et al. 2011](#); [Gonzalez et al. 2011, 2012](#); [Wegg & Gerhard 2013](#); [Wegg et al. 2015](#)). We assume the same stellar parameters for the RBB and AGBB as [Nataf et al. \(2013b\)](#).

We require a dual colour-cut and a magnitude cut on our sample to select the red giant branch:

$$\begin{aligned} (V - I) &\geq (V - I)_{RC} - 0.30, \\ (J - K_s) &\geq (J - K_s)_{RC} - 0.30, \\ |I - I_{RC}| &\leq 1.50, \end{aligned} \quad (5)$$

where the colour-cuts are only applied if the colours are measured. The fit is repeated until the guessed parameters agree with the output parameters⁴ to 0.03 mag in $(V - I)$ and 0.10 mag in I . The relatively weak Gaussian priors in the parameters A , B , and N_{RC} :

$$\begin{aligned} B &\sim \mathcal{N}(0.55, 0.03) \\ N_{RC}/A &\sim \mathcal{N}(1.17, 0.07), \end{aligned} \quad (6)$$

⁴ The condition is relaxed to 0.04 mag if $(V - I)_{RC} \geq 3.20$.

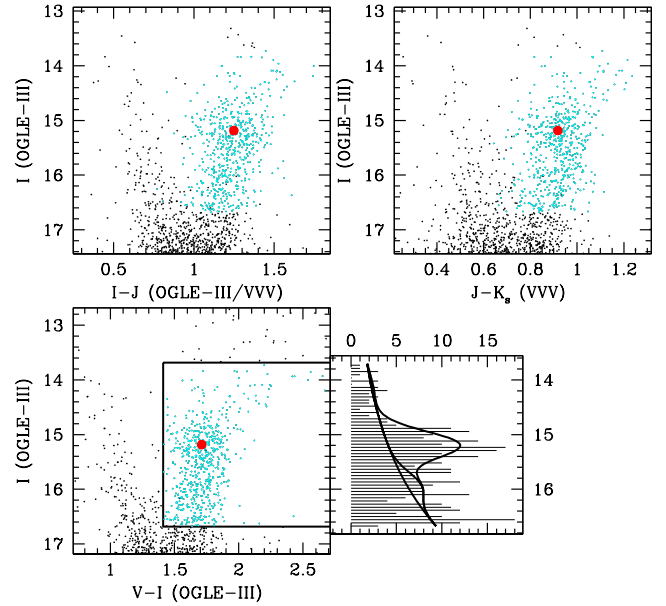


Figure 2. Colour-magnitude diagrams in I vs $(I - J, J - K_s, V - I)$ toward $(l, b) = (2.94^\circ, +3.06^\circ)$, with a luminosity function and best-fit model in the histogram. The cyan dots are those over which the fit is performed, and the black dots are the entire detected colour-magnitude diagram. The three measured colours of the red clump, delineated by the red dots, are well-measured in all three colour-magnitude diagrams.

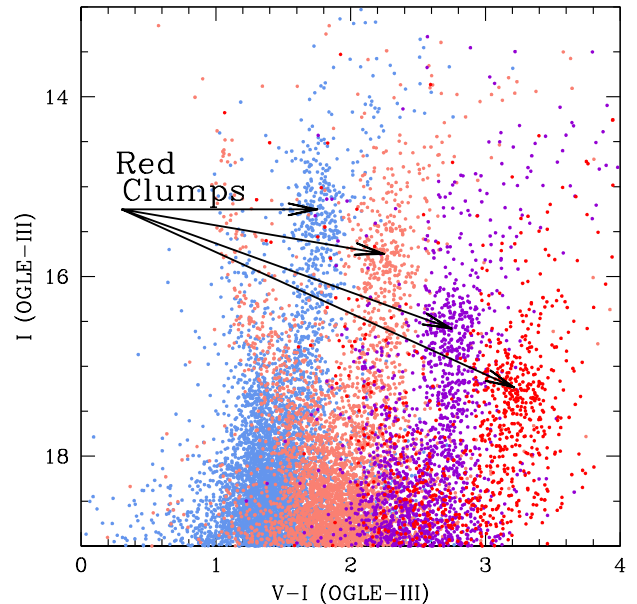


Figure 3. I vs $(V - I)$ colour-magnitude diagrams of four red giant branches with red clump colours of $(V - I)_{RC} = 1.76, 2.25, 2.75$, and 3.22 . Reddening and extinction are clearly quantities that can be precisely measured.

are imposed to increase stability of the fit and, thus, reduce the scatter in the derived value of I_{RC} . The three RC colours $(V-I)_{RC}$, $(I-J)_{RC}$, and $(J-K_s)_{RC}$ are determined independently, by picking the colour that minimizes the dispersion in colour at the luminosity of the RC. A demonstration of the colour and magnitude determinations is shown in Figure 2. We show four fields with four different reddening values in Figure 3.

A difficulty with our study, not shared by most previous photometric bulge studies, are the different sensitivities of the *VVV* and *OGLE-III* datasets. The near-IR dataset probes further down the luminosity function in highly-reddened fields. Nataf et al. (2013b) excluded sightlines with $(V-I)_{RC} \geq 3.30$ for that reason, as V magnitudes of stars located in the color-magnitude diagrams close to the RC were at or below the detection limit in *OGLE* dataset for reddening values $(V-I)_{RC} \geq 3.30$. In this investigation, in order to be able to include also such highly reddened sightlines, we fit the $(V-I)$ vs $(I-K_s)$ colour-colour relations for stars slightly brighter and redder than the RC, satisfying $0.50 \leq I_{RC} - I \leq 2.0$ and $0 \leq (I-K_s) - (I-K_s)_{RC} \leq 0.70$. The fit is only applied to stars redder than the RC (observationally, not intrinsically), to avoid contamination from foreground disk stars that would have lower mean reddening, and thus shifted colour-colour terms. The intercept to the colour-colour relations is used for sightlines where the intercept satisfied $(V-I)_{RC} \geq 3.20$. There is a systematic shift of 0.0413 mag between the intercept to the colour-colour relations and the RC colour determined in the standard way, plausibly due to a gravity term in the colour-colour relations. This shift is measured from sightlines where $2.40 \leq (V-I)_{RC} \leq 3.20$, and applied to more reddened sightlines, $(V-I)_{RC} \geq 3.20$.

4 THE EXTINCTION CURVE IN $VIJK_s$: THEORETICAL EXPECTATIONS

In this section we list the predicted extinction coefficients of Cardelli et al. (1989), Fitzpatrick (1999), and Fitzpatrick & Massa (2007), given the filter transmission function of the photometric systems studied in this work, a RC model atmosphere, and typical extinction values. For the extinction curve of Fitzpatrick & Massa (2007), we only show the $R_V = 3.001$ which is their mean Galactic extinction curve – no general formalism is provided in that work for capturing the effect of R_V variations across the full wavelength range, deliberate on the part of the authors.

In Table 2 we show the predicted extinction coefficients as per a variety of assumptions. We list the broadband extinctions as ratios relative to A_{5500} , which is the hypothetical extinction one would measure in a narrow-band filter placed at 5500 Å (very close but not identical to the Landolt V -band filter), a definition chosen to avoid ambiguities with respect to A_V or $E(B-V)$. We find that what affects the extinction coefficients a great deal are the underlying parameterization (i.e. the chosen reference) and the choice of R_V value. The convolution with the extinction curve itself has little impact, and thus extinction coefficients can be assumed to be independent of extinction. The ratio $E(V-I)/A_{5500}$, where A_{5500} is the extinction at 5500 Å, is predicted to shrink by $\sim 0.75\%$ or 0.003 as A_V is doubled. Though there are

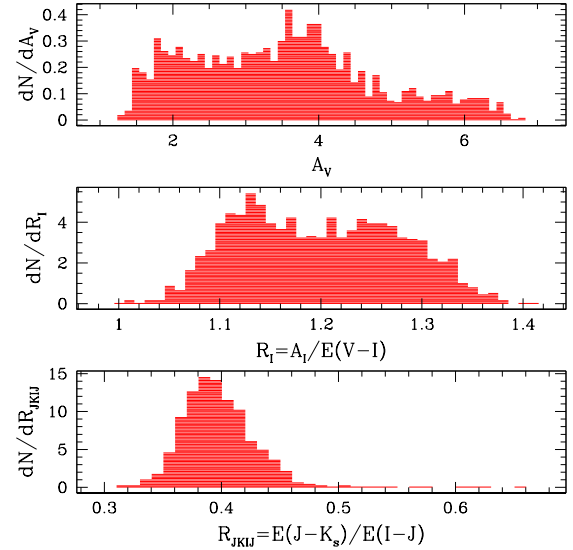


Figure 4. Distributions of the extinction A_V and the reddening ratios $A_I/E(V-I)$ and $E(J-K_s)/E(I-J)$ as measured in our study.

contexts where this will matter, an offset of ~ 0.01 mag in $E(V-I)$ is too small to affect any of the conclusions reached in this work. We also list the predicted extinction coefficients for the spectra of a typical RR Lyrae star, they are nearly identical to those of RC stars, and thus studies of RR Lyrae stars and RC stars should yield consistent answers for the photometric filters used here.

5 RESULTS

We show in Figure 4 the distribution of the extinction A_V , and the reddening ratios $A_I/E(V-I)$ and $E(J-K_s)/E(I-J)$ as measured toward our 1,854 sightlines satisfying each of the photometric completeness criterion $(V-I)_{RC} \leq 4.30$, and the two differential reddening criteria $\sigma_{I,RC} \leq 0.30$ and $\sigma_{(V-I)_{RC}} \leq 0.18$. We obtain a broad distribution in each of these parameters, demonstrating our sensitivity to variations in the input parameter space. Specific findings are discussed below. The full list of values derived is available in Table 3.

5.1 The Extinction Curve is Variable

We confirm a result of Udalski (2003b), Gosling et al. (2009), and Nataf et al. (2013b), that the extinction curve toward the inner Milky Way is variable.

In the left panel Figure 5, we show the CMDs for two sightlines which have $E(V-I)$ values that agree to ~ 0.02 mag, suggesting that they have the “same reddening”. They do not, that similarity in $E(V-I)$ is due to a fortuitous cancellation between the types and quantities of dust toward those two sightlines. Though the $E(V-I)$ values agree, the $E(J-K_s)$ values differ by 0.28 mag, corresponding to 65%. These variations are significant, and large, and thus need to be accounted for in any rigorous study of bulge photometric temperatures, metallicities, or other stellar parameters. The

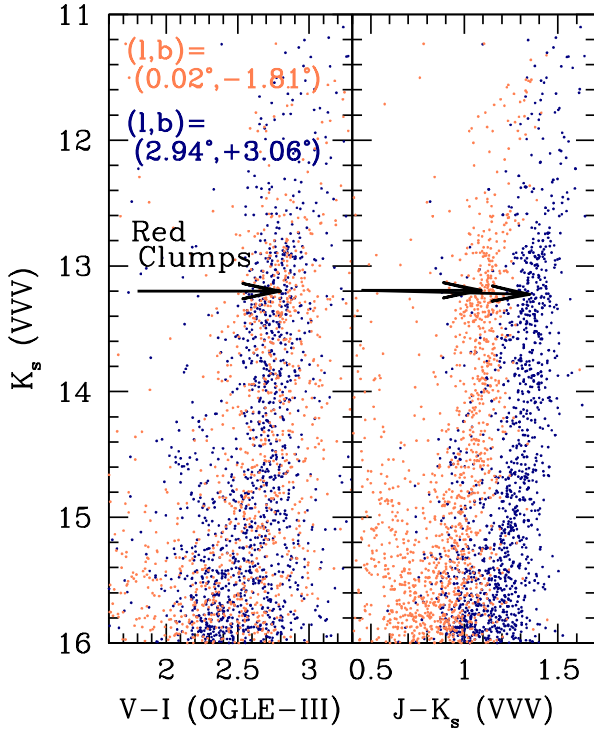


Figure 5. Colour-magnitude diagrams of two bulge sightlines demonstrating the variable extinction curve. The $(V - I)_{RC}$ colours of the two sightlines agree to ~ 0.02 mag, yet their $(J - K_s)_{RC}$ differ by ~ 0.28 mag, thus demonstrating a variation in the extinction curve. The extinction toward one sightline goes as $E(J - K_s)/E(V - I) = 0.26$ (orange dots), whereas that toward the other goes as $E(J - K_s)/E(V - I) = 0.41$ (blue dots).

differences in colour cannot be due to differences in the intrinsic stellar populations, as these two sightlines have similar metallicities (Gonzalez et al. 2013), whereas the right panel of Figure 5 shows the $(J - K_s)$ colour distribution of the red giant stars differing not just in the mean, but in fact are completely non-overlapping.

We present the same idea in a different manner in Figure 6. These two sightlines are selected to have nearly equal values of $E(I - J)$, but the sightline with greater $E(J - K_s)$, by 0.21 mag, has an $E(V - I)$ value that is 0.17 mag lower.

5.2 The Extinction Curve is Non-Standard

We show in Figure 7 the scatter of $A_I/E(V - I)$, $E(I - J)/E(J - K_s)$, and $E(J - K_s)/E(V - I)$ relative to one another. These extinction coefficients vary in a correlated manner. We also show the predictions of Cardelli et al. (1989), Fitzpatrick (1999), and Fitzpatrick & Massa (2007), which are obtained by convolving their extinction curves with a synthetic red clump atmospheric spectrum and 4 magnitudes of extinction at 5500 Å, typical of the sightlines investigated in this work.

The comparison to predictions leads to a conclusion that are entirely new to this investigation. Not only the $R_V = 3.1$ curves of Cardelli et al. (1989) and Fitzpatrick (1999) (delineated by the blue and green circles respectively) poor fits

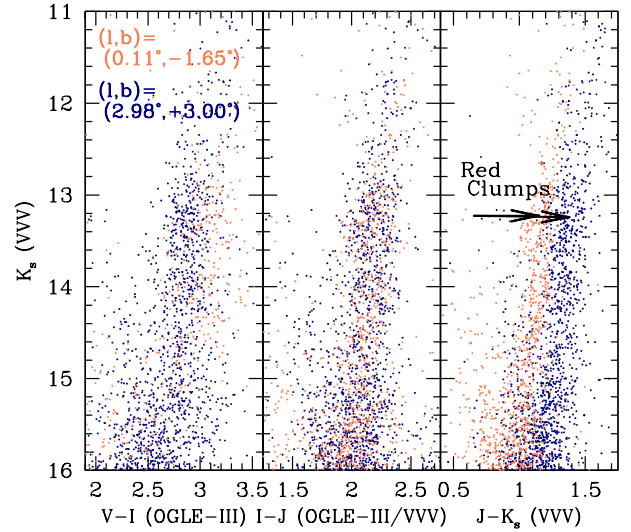


Figure 6. Colour-magnitude diagrams of two bulge sightlines demonstrating the variable extinction curve. The two sightlines are selected to have reddening $E(I - J)$ that agrees to 0.01 mag. However, the sightline with lower reddening $E(V - I)$ by 0.17 mag (blue dots) has higher reddening $E(J - K_s)$ by 0.21 mag.

to the data over the entire span of extinction curves measured toward the bulge, but these parameterizations actually fail to intersect the bulge extinction trends *regardless of how R_V is varied*. Nataf et al. (2013b) claimed that the $R_V \approx 2.5$ extinction curve from Cardelli et al. (1989) was a good fit, as it nearly fit the mean values of $A_I/E(V - I)$ and $E(J - K_s)/E(V - I)$, see the bottom-right panel of Figure 7. However, the addition of the measurement $E(I - J)$ shows that the extinction curves of Cardelli et al. (1989) (and of Fitzpatrick 1999) fail for all values of R_V , not just in the mean, but they fail completely. The blue and green lines *never* intersect the cloud of red points.

A possible explanation for this is that the extinction curve toward the inner Milky Way is in fact standard, but the “standard” is not accurately characterized by the works of Cardelli et al. (1989) and Fitzpatrick (1999), and that studies of the bulge should instead use the mean Galactic extinction curve of Fitzpatrick & Massa (2007) (the magenta square in Figure 7), which benefits from broader and more accurate measurements. The parameterization of Fitzpatrick & Massa (2007) is used by Babusiaux et al. (2014) in their derivation of probabilistic distances to bulge stars.

The mean Galactic extinction curve of Fitzpatrick & Massa (2007) does in fact fare better. However, it is still significantly off the relations. The discrepancy corresponds to an underestimate of 0.016 (1.3%) in the mean value of $A_I/E(V - I)$, an underestimate of 0.089 (12%) in the mean value of $E(I - J)/E(J - K_s)$, and an overestimate of 0.026 (8.9%) in the mean value of $E(J - K_s)/E(V - I)$. However, the mean Galactic extinction curve of Fitzpatrick & Massa (2007) never intersects the trend spanned by the red points, and the offsets will clearly often be larger than the offset to the mean.

Thus, the extinction toward the inner Milky Way, both

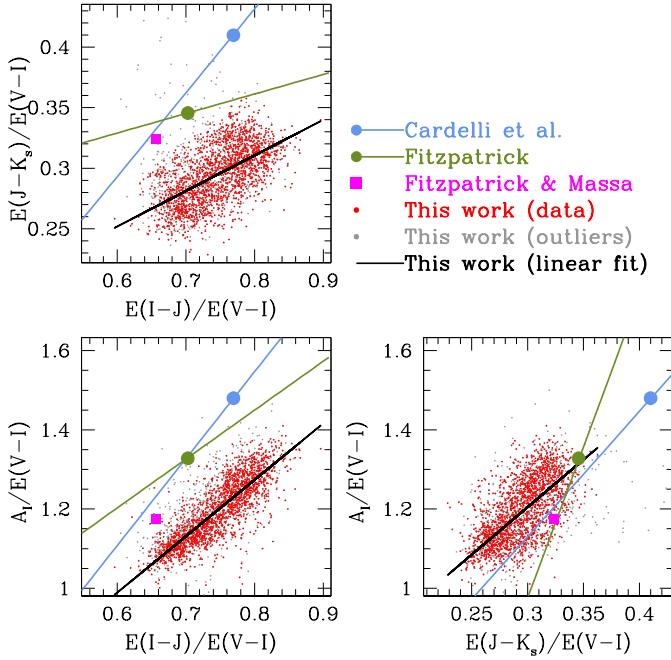


Figure 7. Scatter plots of $A_I/E(V-I)$, $E(I-J)/E(V-I)$, and $E(J-K_s)/E(V-I)$ versus one another. The extinction curves of Cardelli et al. (1989), Fitzpatrick (1999), and Fitzpatrick & Massa (2007) are poor fits to the data both in the mean and in the trend, regardless of how R_V is varied, with the large blue, green, and magenta dot referring to the predicted $R_V = 3.1, 3.1, 3.0$ cases respectively.

the mean curve and the dominant trends in the curve, is not well-fit by the works of Cardelli et al. (1989), Fitzpatrick (1999), and Fitzpatrick & Massa (2007), even allowing for variations in R_V .

5.3 Whither R_V : The Shape of the Extinction Curve Has At Least Two Degrees of Freedom

We show in Figure 8 the distribution of $E(J-K_s)/E(I-J)$ vs $A_I/E(V-I)$ – they appear uncorrelated. A Pearson coefficient for 1,854 measurements satisfying the criteria $(V-I)_{RC} \leq 4.30$, $\sigma_{(V-I)_{RC}} \leq 0.18$, $R_I \leq 1.45$ and $\sigma_{I,RC} \leq 0.30$ yields $\rho = -0.0274$ – effectively zero. As with Figure 7, the observed distribution of extinction curve parameters lies off the relations predicted by Cardelli et al. (1989), Fitzpatrick (1999), and Fitzpatrick & Massa (2007).

That these two ratios have uncorrelated variations disproves the canonical expectation that variations in the shape of the optical+near-IR extinction curve can be explained by a single parameter, R_V . There are at least two independent degrees of freedom in the optical+near-IR wavelength regime, and the fact that the maximum we can possibly measure with four photometric bandpasses is three degrees of freedom, suggests that there may be more.

In Figure 9, we show the distributions of $E(J-K_s)/E(V-I)$ and $A_I/E(V-I)$ as a function of direction. In both cases, adjacent sightlines tend to have similar values of the extinction coefficient, which robustly suggests that the measurements and their variations are significant.

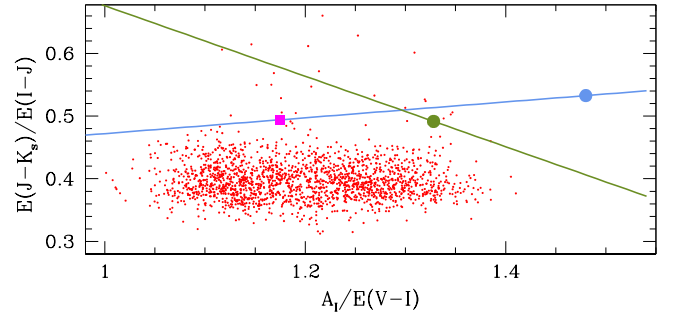


Figure 8. Scatter plots of $E(J-K_s)/E(I-J)$ versus $A_I/E(V-I)$. The extinction curves of Cardelli et al. (1989), Fitzpatrick (1999), and Fitzpatrick & Massa (2007) are poor fits to the data both in the mean and in the trend, regardless of how R_V is varied.

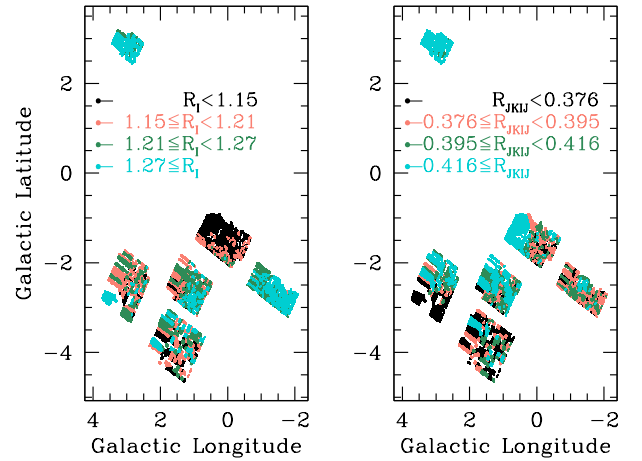


Figure 9. Spatial distribution as a function of Galactic coordinates (degrees) of the optical extinction coefficient $R_I = A_I/E(V-I)$ (left panel) and the near-IR extinction coefficient $R_{JKIJ} = E(J-K_s)/E(I-J)$ (right panel). The colours denote quartiles weighted to have approximately equal surface area. Though both the optical and near-IR extinction coefficients have significant variations across the sky, these variations are uncorrelated.

The distinct distributions in the left and right panels clearly demonstrate that the variations are largely uncorrelated.

Of interest in Figure 8 is a sparse cloud of outliers with much higher values of $E(J-K_s)/E(I-J)$. These points appear spurious at first glance, but they turn out to be legitimate. In Figure 10, we show the CMDs for a sightline toward $(l, b) = (1.68^\circ, -3.58^\circ)$, with measured extinction coefficient of $E(J-K_s)/E(I-J) = 0.66$, vastly higher than the sample mean of $E(J-K_s)/E(I-J) = 0.40$. The CMDs reveal that the sightline looks fine, there's no confounding issue such as neglected removal of globular cluster contamination, differential reddening, or failed colour-selection. We also verify the photometry by comparing the VISTA photometry to the 2MASS photometry for some of the brighter points, to rule out any potential issues with calibration or observational factors such as the passage of small clouds or bright solar system bodies during the VISTA observations.

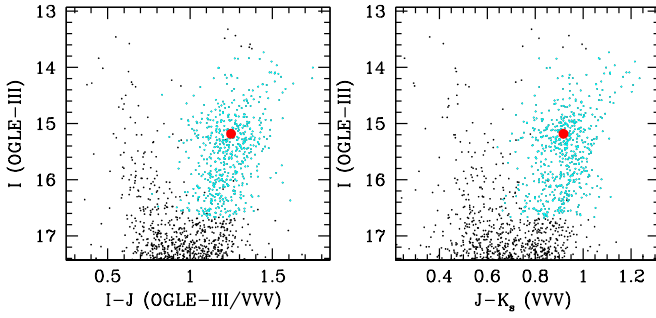


Figure 10. Colour-magnitude diagrams in I vs $(I-J, J-K_s)$ toward $(l, b) = (1.68^\circ, -3.58^\circ)$. Symbols are as in Figure 2. This sightline, with an anomalous large extinction coefficient of $E(J-K_s)/E(I-J) = 0.66$, gives no indication from its CMD of being the product of a systematic such as differential reddening.

In both J and K_s , the differences are usually less than 0.10 mag, and thus the measurements are deemed reliable.

Thus, we have to conclude that the story of extinction curve variations toward the inner Milky Way is a much deeper story than that of R_V variations. Further, the cloud of spurious-looking outliers near the top of Figure 8 is in fact physically significant.

5.4 A Principal Component Analysis of Extinction Coefficient Variations

Principal component analysis (PCA) is a statistical tool to analyze the number of degrees of freedom of a dataset without the possible bias of needing physical interpretation of the meaning of each variable, thus allowing the data to speak for itself. A set of orthogonal basis vectors is computed by rotating the coordinate-axes in which the variables measured in an n -dimensional space (where “ n ” is the number of variables) such that the new variables are uncorrelated (see Andrews et al. 2012 for an astronomy-relevant application).

We compute the principal components over three variables, $0.8352 \times (A_I/E(V-I) - 1.1973)$, $1.3406 \times (E(I-J)/E(V-I) - 0.7459)$, and $3.3822 \times (E(J-K_s)/E(V-I) - 0.2965)$. The coefficients $\{0.8352, 1.3406, 3.3822\}$ are chosen such that each input dimension has the same mean value, otherwise the first principal component will be nearly parallel to the largest vector, whereas we are interested in diagnosing extinction curve variations consistently over the entire wavelength regime. Principal component decomposition automatically subtracts the means of the three vectors: $\{1.1973, 0.7459, 0.2965\}$.

The three eigenvalues of the principal component decomposition are 0.0117, 0.0034, and 0.0008, corresponding to standard deviations along the axes of $\sim(11, 6, 3)\%$ in the three rotated reddening ratios. The three principal components derived contribute 73%, 22%, and 5% of the total variance, consistent with the claim made in the prior section that we find two degrees of freedom to the extinction curve in our dataset. The projection of the reddening vectors onto the principal component space is shown in Figure 11. The

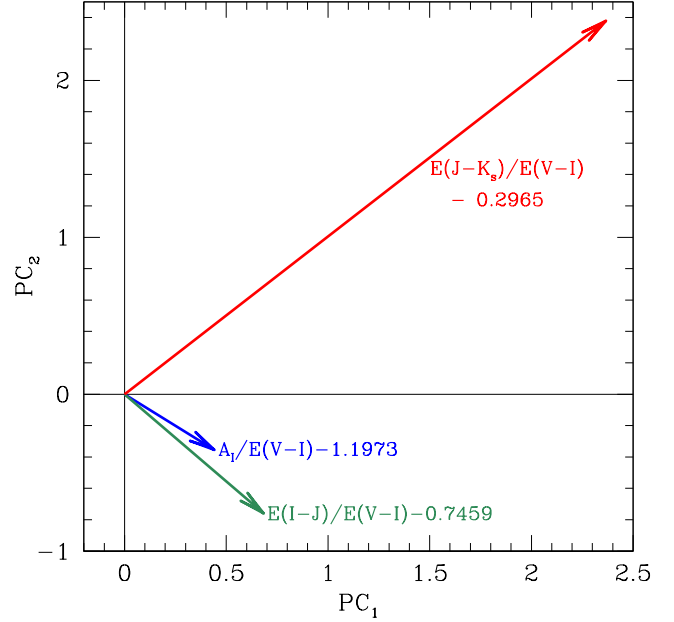


Figure 11. Projection of the three independent extinction ratios onto the plane of the first two principal components. In this parameterization, the lengths of the vectors correspond to the inverse as their average value in our data set. These two principal components describe 73% and 22% of the variance of the three extinction ratios.

first two principal components are equal to:

$$\begin{aligned} PC_1 = & 0.6340(A_I/E(V-I) - 1.1973) \\ & + 0.3555(E(I-J)/E(V-I) - 0.7459) \\ & + 0.2081(E(J-K_s)/E(V-I) - 0.2965) \end{aligned} \quad (7)$$

$$\begin{aligned} PC_2 = & -0.5088(A_I/E(V-I) - 1.1973) \\ & - 0.4229(E(I-J)/E(V-I) - 0.7459) \\ & + 0.2092(E(J-K_s)/E(V-I) - 0.2965) \end{aligned} \quad (8)$$

5.5 Critical Boundary Value: Relative Extinction in V and K_s

We can estimate extinction in different filters with a conversion such as the following:

$$A_{K_s} = A_I - E(I-J) - E(J-K_s). \quad (9)$$

Though Equation 9 has the advantage of being analytically exact, it has the disadvantage of producing extinction measurements with correlated errors, as the error in A_I enters linearly into A_{K_s} , which is why the majority of the analysis in this paper focuses on the (independent) measurements of the colour excesses.

Regardless, the ratios should still be reliable in the median, for which we measure:

$$\left| \frac{A_V}{A_{K_s}} \right| = 13.44. \quad (10)$$

That is a considerably greater ratio than the canonical value of 8.25 (Cardelli et al. 1989). The three median ratios measured in this work, $A_V : A_I : A_J : A_{K_s}$, are

1 : 1.85 : 4.84 : 13.44. We report the median rather than the mean as the mean is distorted by a small number of sightlines with considerable errors, leading to unphysically small values of A_{K_s} .

5.6 Construction of Better Wesenheit Functions to Minimize the Effects of Extinction

In various fields of astronomy such as the cosmological distance ladder, *Wesenheit*⁵ functions are used to minimize the dependence of extinction on apparent magnitudes and thus distances (Madore 1982; Majaess et al. 2011; Shappee & Stanek 2011; Wagner-Kaiser et al. 2015). This is done by subtracting from the apparent magnitude a colour term where the slope is believed to be the average total-to-selective extinction ratio, for example:

$$W_I = I - 1.45(V - I), \quad (11)$$

is commonly used, and has some empirical support toward sightlines such as the LMC (Udalski 2003b; Pejcha & Kochanek 2012). Though Equation 11 no doubt performs very well over large swaths of the sky, we have demonstrated in this work that it fails spectacularly toward the inner Milky Way. We have also demonstrated that there is no single universal extinction curve for this Galaxy, and thus it is safe to assume that the same applies to other galaxies. Thus, such simple Wesenheit functions should usually be done away with in this era of precision cosmology.

An alternative, as per the fits seen in Figure 7, the use of *uber*⁶-*Wesenheit* functions, such that the apparent magnitude is insensitive to not only variations in extinction assuming a mean extinction curve, but also the dominant first-order variations in the extinction curve. We remove sources with high differential reddening ($\sigma_{(V-I)RC} \geq 0.18$), poor fits ($\sigma_{RC} \geq 0.30$), very high-reddening values that increase the odds of potential systematics such as incompleteness ($(V - I)_{RC} \geq 4.30$) and extreme values of the extreme coefficients ($A_I/E(V - I) \geq 1.45$, $E(J - K_s)/E(I - J) \geq 0.46$). We recursively remove 3- σ outliers and obtain the following relation on the VIJ plane:

$$A_I = 0.1333E(V - I) + 1.4254E(I - J) \quad (12)$$

It is a tighter relation, with a correlation coefficient $\rho = 0.8194$, and can also be discerned from Figure 7. A serendipitous result emerges: the coefficient of $E(V - I)$ is very small, only 9% the size of the coefficient of $E(I - J)$. In practice, it turns out that the total-to-selective extinction ratio $A_I/E(I - J)$ has very little dependence on extinction curve variations. The mean value is given by $\langle A_I/E(I - J) \rangle = 1.6063$, and the 1- σ scatter by $\sigma_{A_I/E(I - J)} = 0.066$, or 4.1%. In contrast, the scatter we expect just from the statistical measurement error in I_{RC} is 2.3%, and thus the intrinsic scatter in $A_I/E(I - J)$ is as small as 3.4% in our sample.

We thus suggest:

$$W_I = I - 1.61(I - J), \quad (13)$$

as a surprisingly robust Wesenheit magnitude. We note that the predicted extinction coefficients of $A_I/E(I - J)$

J) from Cardelli et al. (1989), Fitzpatrick (1999), and Fitzpatrick & Massa (2007) are 1.93, 1.89, and 1.79 respectively.

6 COMPARISONS TO PRIOR INVESTIGATIONS

6.1 Shorter-Wavelength Photometry

In principle it would be interesting to map extinction curve variations over the broadest possible wavelength, which should become possible over time as more photometry of the Galactic bulge is taken.

One study available for comparison is that of Revnivtsev et al. (2010), who measured photometry of the “Chandra bulge field” (toward $(l, b) = (0.11^\circ, -1.43^\circ)$) in a diverse array of filters with HST’s *Advanced Camera for Surveys* (ACS). Unfortunately, we cannot make a direct comparison as they did not publish their input data, only their final results. They report $A_{F625W,ACS}/(A_{F435W,ACS} - A_{F625W,ACS}) = 1.25 \pm 0.09$. Their error was the uncertainty on the regression, which emerges due to both measurement errors and the genuine variations in the underlying extinction curve. Given the latter source of error, their quoted error is actually likely to be an overestimate. The predicted coefficients from standard extinction curves of Cardelli et al. (1989), Fitzpatrick (1999), and Fitzpatrick & Massa (2007) are approximately 1.92, 1.64, and 1.64 respectively. Revnivtsev et al. (2010) thus measured a steeper-than-standard extinction curve toward those sightlines, regardless of how one defines “standard”. The predicted extinction curves are either $R_V = 1.97$ (Cardelli et al. 1989) or $R_V = 2.46$ (Fitzpatrick 1999).

The typical extinction coefficients we measure toward those sightlines are $A_I/E(V - I) = 1.10$, $E(I - J)/E(V - I) = 0.70$, and $E(J - K_s)/E(V - I) = 0.25$. Interestingly, we cannot find an R_V match even if we restrict the fit to the optical filters. Fitting $A_I/E(V - I) = 1.10$ requires $R_V \approx 2.20$ in either the parameterization of Cardelli et al. (1989) or that of Fitzpatrick (1999). The resulting predicted values of $A_{F625W,ACS}/(A_{F435W,ACS} - A_{F625W,ACS})$ are 1.39 and 1.09 respectively, both failing to match the result of Revnivtsev et al. (2010), with equal errors of opposite signs. We list all of the implied values of R_V toward this sightline in Table 4.

6.2 Measurements of Diffuse Interstellar Bands

The correlation between the diffuse interstellar band located at $\lambda_0 = 15272.42 \text{ \AA}$ and interstellar reddening was measured by Zasowski et al. (2015):

$$\langle W_{DIB} \rangle = 12.2572 * E(H - [4.5\mu]), \quad (14)$$

where W_{DIB} is the diffuse interstellar band equivalent width in milli-angstroms, and the reddening $E(H - [4.5\mu])$ is taken from Nidever et al. (2012). The function reported by Zasowski et al. (2015) is in terms of A_V , which was extracted from the measurements of Majewski et al. (2011) with the conversion factors $A_V = 8.8A_{K_s}$, $A_{K_s} = 0.918E(H - [4.5\mu])$.

We match our catalogue of reddening and extinction curve variations with that of W_{DIB} and $E(H -$

⁵ “Wesenheit” is the German word for “essence” or “nature”.

⁶ “uber” is the German word for “above” or “at a higher level”.

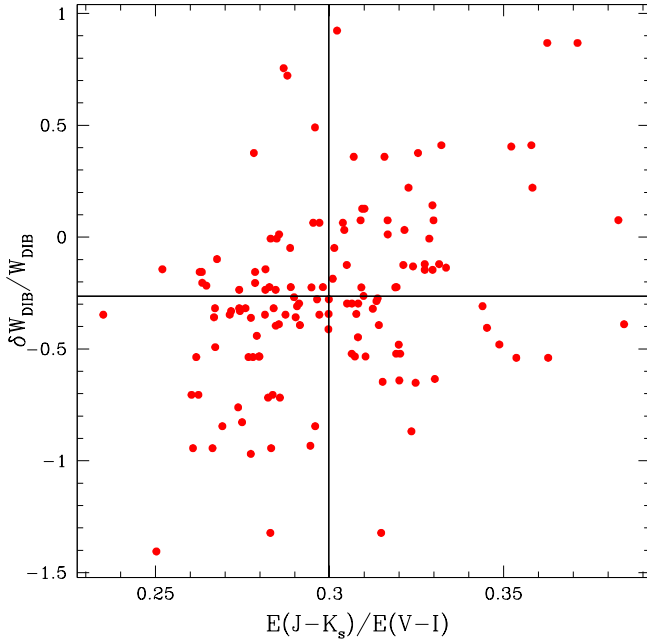


Figure 12. Scatter of residual of diffuse interstellar band strength relative to predictions of Zasowski et al. (2015), versus the $E(J - K_s)/E(V - I)$ measurements from Nataf et al. (2013b), shown as red points. There is a slight, positive correlation, $\rho = +0.34$. The thick black lines denote the mean values of the two variables for the 137 data points. The mean $1\text{-}\sigma$ measurement error in $\delta W_{DIB}/W_{DIB}$ is 0.27.

$[4.5\mu]$ measurements satisfying ($|l| \leq 5^\circ$, $|b| \leq 5^\circ$) from Zasowski et al. (2015). We obtain a paltry 23 matches, due to poor spatial overlap. In order to expand the sample, we match the DIB catalogue of Zasowski et al. (2015) to the $E(J - K_s)/E(V - I)$ catalogue of Nataf et al. (2013b), which is the extinction ratio most reliably measured in that work. This yields 137 matches.

Then, from each W_{DIB} measurement, we subtract the predicted measurement to obtain a residual:

$$\frac{\delta W_{DIB}}{W_{DIB}} = \frac{W_{DIB} - 12.2572 * E(H - [4.5\mu])}{W_{DIB}}. \quad (15)$$

One might expect the residuals to be randomly distributed and have a mean of zero. However, we instead find a correlation of $\rho = +0.34$ between $\delta W_{DIB}/W_{DIB}$ and $E(J - K_s)/E(V - I)$. We show the scatter in Figure 12. The p-value for the correlation is 4.6×10^{-5} – the odds of deriving this correlation by chance are $\sim 21,000:1$.

Interestingly, the mean value in $\delta W_{DIB}/W_{DIB}$ is -0.26 . This is extremely unlikely to be due to chance as the scatter measured by Zasowski et al. (2015) was $\sim 50\%$ per star, and thus our sample mean is a $\sim 6.2\sigma$ outlier. This offset is consistent with the accumulating evidence that the interstellar medium toward the inner Milky Way has systematically different properties to that elsewhere in the Galaxy. The correlation between $E(J - K_s)/E(V - I)$ and $\delta W_{DIB}/W_{DIB}$ implies a “standard” value of $\delta W_{DIB}/W_{DIB}$ would be reached in the mean if a “standard” value of $E(J - K_s)/E(V - I)$ is also reached in the mean.

This suggests that the ratio between diffuse interstellar

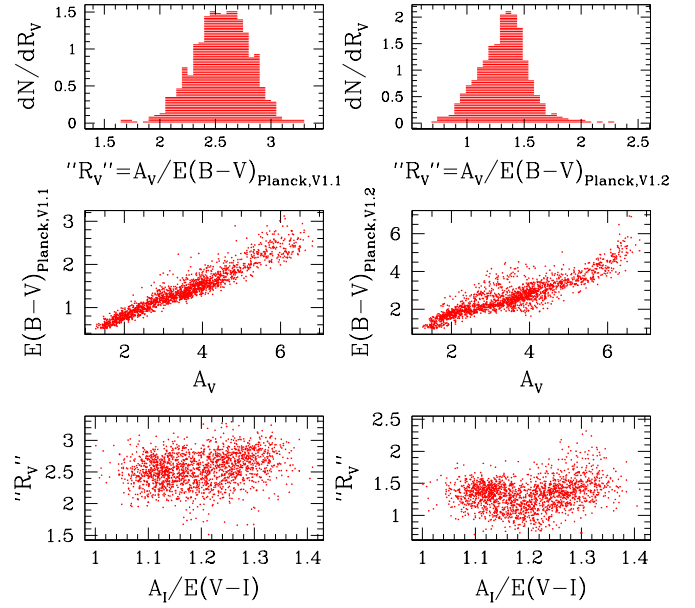


Figure 13. *Planck* determinations of $E(B - V)$ from the version 1.1 maps (left panels) and 1.2 maps (right panels) as a function of A_V in the top and middle panels, and $A_I/E(B - V)$ in the bottom panels. The version 1.1 maps do better in the mean than the version 1.2 maps. Neither version appears sensitive to extinction curve variations.

band strength and interstellar extinction may depend on the properties of interstellar medium. This is not surprising, given observations of sightline dependence for other diffuse interstellar bands (Kos & Zwitter 2013), though it is the first demonstration for the $\lambda_0 = 15272.42 \text{ \AA}$ diffuse interstellar band. This issue warrants further investigation. We point to the recent measurement of five distinct diffuse interstellar band equivalent widths toward the type Ia supernova 2014J by Jack et al. (2015), which is located behind anomalous dust (Goobar et al. 2014), as an example of potential future applications.

6.3 The Planck Reddening Maps

We compare our reddening measurements to the version 1.1 $E(B - V)$ all-sky maps from *Planck*, and the version 1.2 maps (Planck Collaboration et al. 2014). The *Planck* maps report $E(B - V)$, which we can compare to our measurements of A_V to obtain a fiducial R_V . We show various diagnostics in Figure 13. We find that neither reddening map works well, both have unexplained scatter, but the bias in the version 1.2 maps relative to the measured reddening reaching a catastrophic and colossal $\sim 100\%$.

The version 1.1 maps (left panels) yield a mean and standard deviation of $R_V = 2.55 \pm 0.25$, both plausible given the other measurements in this work. However, in the bottom panel we see that the suggested R_V is uncorrelated with $A_I/E(V - I)$ ($\rho = 0.25$), with the correlation dropping to $\rho = 0.20$ and $\rho = 0.03$ for $E(I - J)/E(V - I)$ and $E(J - K_s)/E(V - I)$ respectively. In contrast, the correlations between $A_I/E(V - I)$ and $E(I - J)/E(V - I)$ and $E(J - K_s)/E(V - I)$ were $\rho = 0.80$ and $\rho = 0.57$, respec-

tively, see Figure 7. The fact that all of these correlations are small suggests that extinction curve variations are not responsible for the offset between reddenings inferred from infra-red emission and that measured from stellar colours, and that there is another source of “error” at play.

The version 1.2 maps (right panels of Figure 13) yield a mean and standard deviation of $R_V = 1.33 \pm 0.22$, which is not plausible given the other measurements in this work, and suggests that reddening in the version 2 maps is overestimated by a factor of 2. In the bottom panel we see that the suggested R_V is uncorrelated with $A_I/E(V-I)$ ($\rho = 0.20$), which seems unlikely, though it would be beneficial to obtain B -band photometry of the bulge in order to be sure. It also appears to have a strange quadratic behaviour, with R_V minimized at $A_I/E(V-I) \approx 1.20$, approximately the mean value in our sample.

The effect of background extinction, whereby emission from dust located behind the red clump stars, could in principal be a potential bias to the results. However, we expect to be small, as our sightlines typically intersect the bulge at a height ~ 300 pc above the plane. We measure the Pearson correlation coefficient between the ratio of measured reddening $E(V-I)$ and $E(B-V)$ from the Planck v1.1 maps to absolute latitude (a proxy for separation from the plane) to be $\rho = +0.052$, i.e.:

$$\rho\left(\frac{E(V-I)}{E(B-V)_{\text{Planck v1.1}}}, |b|\right) = +0.052. \quad (16)$$

The Pearson correlation coefficient if we instead use the Planck v1.2 maps is $\rho = -0.147$. If background emission were a significant source of error in the analysis, then the ratio of measured to expected reddening would drop rapidly with decreasing absolute latitude, in other words there would be a strong positive correlation. We do not find a large, positive value of ρ with either map, in agreement with our expectation that the systematic error from background emission is small.

The non-linearities that Wolf (2014) identified when comparing the *Planck* reddening maps to photometry of QSOs are not present in our comparison, furthering the argument that they are due to zero point calibrations. Our methodology will necessarily be less sensitive to zero-point calibrations, as the reddening values probed in this work are $\sim 10\times$ higher than those probed by Wolf (2014). What is consistent between our two works are that the version 1.1 map is accurate in the mean whereas the version 1.2 map overestimate reddening by a factor ~ 2 . This consistency is impressive given the different methodology: Wolf (2014) used *ugriz* photometry to study reddening toward QSOs in halo sightlines spanning $\sim 10,000$ deg², and thus probed dust predominantly from the solar neighbourhood, with a normalization of $E(B-V) \lesssim 0.20$.

These discrepancies will ultimately require more resolution, more wavelength coverage and superior comparison with models to resolve. Of possible interest may be the dust model of Jones et al. (2013), which incorporate different distributions of small carbon grains and larger silicate/iron grains.

7 SUMMARY

In this investigation we have combined *VIJK_s* photometry from the OGLE-III and VVV surveys to make nearly 2,000 independent measurements of each of A_I , $E(V-I)$, $E(I-J)$, and $E(J-K_s)$ toward the bulge. We have done so over a range of coordinates within which metallicity variations are small, and for which distance effects due to the Galactic bar can be accounted for.

We confirm previous reports that the extinction curve toward the inner Milky Way is variable and non-standard (Udalski 2003b; Gosling et al. 2009; Nataf et al. 2013b). Furthermore, not only is the extinction curve non-standard in the mean, it is also poorly fit by the parameterizations of Cardelli et al. (1989) and Fitzpatrick (1999) regardless of how R_V is varied. The mean Galactic extinction curve of Fitzpatrick & Massa (2007) is also a poor fit. These fits are poor both with respect to the mean of the Galactic bulge extinction curve, as well as the fact they never intersect the variations thereof.

We find that the shape of the interstellar extinction has at least two degrees of freedom, as the variations in $A_I/E(V-I)$ and $E(J-K_s)/E(I-J)$ are uncorrelated. We use principal component analysis to confirm the presence of two significant independent degrees of freedom in our data. This suggests a relatively large, and completely undiagnosed, source of systematic errors in cosmological investigations of Cepheids and Type Ia supernovae.

We look forward to extending our investigations over a broader range of wavelengths, for example by incorporating photometry from the Dark Energy Camera (DePoy et al. 2008) and Pan-STARRS (Tonry et al. 2012). Further insights may be gleaned by comparison to measurements of diffuse interstellar bands from surveys such as APOGEE (Zasowski et al. 2015, a comparison already begun in this work) GALAH (De Silva et al. 2015), and Gaia-ESO (Pushtarini et al. 2015).

8 ACKNOWLEDGMENTS

We thank the referee for a helpful review of the manuscript.

We thank Andrew Gould, Carine Babusiaux, Albert Zijlstra, and Edward Schlafly for helpful discussions.

D.M.N. was primarily supported by the Australian Research Council grant FL110100012. This research was supported in part by the National Science Foundation under Grant No. NSF PHY11-25915.

The OGLE project has received funding from the National Science Centre, Poland, grant MAESTRO 2014/14/A/ST9/00121 to AU.

We gratefully acknowledge the use of data from the ESO Public Survey program ID 179.B-2002 taken with the VISTA telescope, data products from the Cambridge Astronomical Survey Unit. Support for the authors is provided by the BASAL CATA Center for Astrophysics and Associated Technologies through grant PFB-06, and the Ministry for the Economy, Development, and Tourism’s Programa Iniciativa Científica Milenio through grant IC120009, awarded to Millenium Institute of Astrophysics (MAS). D.M. and M.Z. acknowledge support from FONDECYT Regular grant No. 1130196 and 1150345, respectively. R.K.S. acknowledges

support from CNPq/Brazil through projects 310636/2013-2 and 481468/2013-7. J. A.-G. acknowledges support from Fondecyt Postdoctoral project 3130552 and FIC-R Fund project 30321072

This publication makes use of data products from the Two Micron All Sky Survey, which is a joint project of the University of Massachusetts and the Infrared Processing and Analysis Center/California Institute of Technology, funded by the National Aeronautics and Space Administration and the National Science Foundation.

REFERENCES

- Alonso-García J., Mateo M., Sen B., Banerjee M., Catelan M., Minniti D., von Braun K., 2012, *AJ*, **143**, 70
- Alonso-García J., Dékány I., Catelan M., Contreras Ramos R., Gran F., Amigo P., Leyton P., Minniti D., 2015, *AJ*, **149**, 99
- Altavilla G., et al., 2004, *MNRAS*, **349**, 1344
- Andrews B. H., Weinberg D. H., Johnson J. A., Bensby T., Feltzing S., 2012, *Acta. Astronom.*, **62**, 269
- Babusiaux C., et al., 2014, *A&A*, **563**, A15
- Bachelet E., et al., 2012, *A&A*, **547**, A55
- Bensby T., et al., 2013, *A&A*, **549**, A147
- Bovy J., Rix H.-W., 2013, *ApJ*, **779**, 115
- Bragaglia A., Sneden C., Carretta E., Gratton R. G., Lucatello S., Bernath P. F., Brooke J. S. A., Ram R. S., 2014, *ApJ*, **796**, 68
- Brogaard K., Bruntt H., Grundahl F., Clausen J. V., Frandsen S., Vandenberg D. A., Bedin L. R., 2011, *A&A*, **525**, A2
- Brogaard K., et al., 2012, *A&A*, **543**, A106
- Burns C. R., et al., 2014, *ApJ*, **789**, 32
- Cao L., Mao S., Nataf D., Rattenbury N. J., Gould A., 2013, *MNRAS*, **434**, 595
- Cardelli J. A., Clayton G. C., Mathis J. S., 1989, *ApJ*, **345**, 245
- Casagrande L., Vandenberg D. A., 2014, *MNRAS*, **444**, 392
- Chatzopoulos S., Fritz T. K., Gerhard O., Gillessen S., Wegg C., Genzel R., Pfuhl O., 2015, *MNRAS*, **447**, 948
- Chotard N., et al., 2011, *A&A*, **529**, L4
- Clarkson W. I., et al., 2011, *ApJ*, **735**, 37
- Cordier D., Pietrinferni A., Cassisi S., Salaris M., 2007, *AJ*, **133**, 468
- Cunha K., et al., 2015, *ApJ*, **798**, L41
- Dalton G. B., et al., 2006, in Society of Photo-Optical Instrumentation Engineers (SPIE) Conference Series. p. 0, doi:10.1117/12.670018
- De Silva G. M., et al., 2015, *MNRAS*, **449**, 2604
- DePoy D. L., et al., 2008, in Society of Photo-Optical Instrumentation Engineers (SPIE) Conference Series. p. 0, doi:10.1117/12.789466
- Dong H., et al., 2014, *ApJ*, **785**, 136
- Dwek E., et al., 1995, *ApJ*, **445**, 716
- Emerson J. P., Sutherland W. J., 2010, in Society of Photo-Optical Instrumentation Engineers (SPIE) Conference Series. p. 6, doi:10.1117/12.857105
- Emerson J. P., et al., 2004, in Quinn P. J., Bridger A., eds, Society of Photo-Optical Instrumentation Engineers (SPIE) Conference Series Vol. 5493, Optimizing Scientific Return for Astronomy through Information Technologies. pp 401–410, doi:10.1117/12.551582
- Fausnaugh M. M., Kochanek C. S., Gerke J. R., Macri L. M., Riess A. G., Stanek K. Z., 2015, *MNRAS*, **450**, 3597
- Fitzpatrick E. L., 1999, *PASP*, **111**, 63
- Fitzpatrick E. L., Massa D., 2007, *ApJ*, **663**, 320
- Fitzpatrick E. L., Massa D., 2009, *ApJ*, **699**, 1209
- Fritz T. K., et al., 2011, *ApJ*, **737**, 73
- Gonzalez O. A., Rejkuba M., Zoccali M., Valenti E., Minniti D., 2011, *A&A*, **534**, A3
- Gonzalez O. A., Rejkuba M., Zoccali M., Valenti E., Minniti D., Schultheis M., Tobar R., Chen B., 2012, *A&A*, **543**, A13
- Gonzalez O. A., Rejkuba M., Zoccali M., Valenti E., Minniti D., Tobar R., 2013, *A&A*, **552**, A110
- Goobar A., et al., 2014, *ApJ*, **784**, L12
- Gosling A. J., Bandyopadhyay R. M., Blundell K. M., 2009, *MNRAS*, **394**, 2247
- Gustafsson B., Edvardsson B., Eriksson K., Jørgensen U. G., Nordlund Å., Plez B., 2008, *A&A*, **486**, 951
- Hambly N. C., Mann R. G., Bond I., Sutorius E., Read M., Williams P., Lawrence A., Emerson J. P., 2004, in Quinn P. J., Bridger A., eds, Society of Photo-Optical Instrumentation Engineers (SPIE) Conference Series Vol. 5493, Optimizing Scientific Return for Astronomy through Information Technologies. pp 423–431, doi:10.1117/12.551623
- Henderson C. B., Gaudi B. S., Han C., Skowron J., Penny M. T., Nataf D., Gould A. P., 2014, *ApJ*, **794**, 52
- Hill V., et al., 2011, *A&A*, **534**, A80
- Howes L. M., et al., 2014, *MNRAS*, **445**, 4241
- Howes L. M., et al., 2015, preprint, (arXiv:1511.03930)
- Irwin M. J., et al., 2004, in Quinn P. J., Bridger A., eds, Society of Photo-Optical Instrumentation Engineers (SPIE) Conference Series Vol. 5493, Optimizing Scientific Return for Astronomy through Information Technologies. pp 411–422, doi:10.1117/12.551449
- Jack D., et al., 2015, *MNRAS*, **451**, 4104
- Jones A. P., Fanciullo L., Köhler M., Verstraete L., Guillet V., Bocchio M., Ysard N., 2013, *A&A*, **558**, A62
- Jones D. O., Riess A. G., Scolnic D. M., 2015, *ApJ*, **812**, 31
- Kos J., Zwitter T., 2013, *ApJ*, **774**, 72
- Kunder A., Popowski P., Cook K. H., Chaboyer B., 2008, *AJ*, **135**, 631
- Kunder A., et al., 2015, *ApJ*, **808**, L12
- Landolt A. U., 1992, *AJ*, **104**, 340
- Madore B. F., 1982, *ApJ*, **253**, 575
- Majaess D., Turner D., Gieren W., 2011, *ApJ*, **741**, L36
- Majewski S. R., Zasowski G., Nidever D. L., 2011, *ApJ*, **739**, 25
- Massari D., et al., 2012, *ApJ*, **755**, L32
- Minniti D., et al., 2010, *NewA*, **15**, 433
- Minniti D., et al., 2014, *A&A*, **571**, A91
- Nataf D. M., 2015, *MNRAS*, **449**, 1171
- Nataf D. M., Udalski A., Gould A., Pinsonneault M. H., 2011, *ApJ*, **730**, 118
- Nataf D. M., Gould A. P., Pinsonneault M. H., Udalski A., 2013a, *ApJ*, **766**, 77
- Nataf D. M., et al., 2013b, *ApJ*, **769**, 88
- Nataf D. M., Cassisi S., Athanassoula E., 2014, *MNRAS*, **442**, 2075
- Nataf D. M., et al., 2015, *MNRAS*, **447**, 1535
- Neckel T., Klare G., Sarcander M., 1980, *A&AS*, **42**, 251
- Ness M., et al., 2013, *MNRAS*, **430**, 836
- Nidever D. L., Zasowski G., Majewski S. R., 2012, *ApJS*, **201**, 35
- Nishiyama S., Tamura M., Hatano H., Kato D., Tanabé T., Sugitani K., Nagata T., 2009, *ApJ*, **696**, 1407
- Pejcha O., Kochanek C. S., 2012, *ApJ*, **748**, 107
- Phillips M. M., et al., 2013, *ApJ*, **779**, 38
- Pietrinferni A., Cassisi S., Salaris M., Castelli F., 2004, *ApJ*, **612**, 168
- Pietrukowicz P., et al., 2012, *ApJ*, **750**, 169
- Pietrukowicz P., et al., 2015, *ApJ*, **811**, 113
- Planck Collaboration et al., 2014, *A&A*, **571**, A11
- Portail M., Wegg C., Gerhard O., Martínez-Valpuesta I., 2015, *MNRAS*, **448**, 713
- Pottasch S. R., Bernard-Salas J., 2013, *A&A*, **550**, A35
- Pottasch S. R., Zijlstra A. A., 1994, *A&A*, **289**, 261
- Puspitarini L., et al., 2015, *A&A*, **573**, A35

Revnivtsev M., van den Berg M., Burenin R., Grindlay J. E., Karasev D., Forman W., 2010, *A&A*, **515**, A49

Rich R. M., Origlia L., Valenti E., 2012, *ApJ*, **746**, 59

Riess A. G., et al., 2011, *ApJ*, **730**, 119

Riess A. G., Fliri J., Valls-Gabaud D., 2012, *ApJ*, **745**, 156

Rigault M., et al., 2015, *ApJ*, **802**, 20

Rojas-Arriagada A., et al., 2014, *A&A*, **569**, A103

Ruffle P. M. E., Zijlstra A. A., Walsh J. R., Gray M. D., Gesicki K., Minniti D., Comeron F., 2004, *MNRAS*, **353**, 796

Saito R. K., et al., 2012, *A&A*, **537**, A107

Saracino S., et al., 2015, *ApJ*, **806**, 152

Sarajedini A., et al., 2007, *AJ*, **133**, 1658

Schechter P. L., Mateo M., Saha A., 1993, *PASP*, **105**, 1342

Schlafly E. F., Finkbeiner D. P., 2011, *ApJ*, **737**, 103

Schultheis M., et al., 2014, *AJ*, **148**, 24

Scolnic D. M., Riess A. G., Foley R. J., Rest A., Rodney S. A., Brout D. J., Jones D. O., 2014, *ApJ*, **780**, 37

Shappee B. J., Stanek K. Z., 2011, *ApJ*, **733**, 124

Skrutskie M. F., et al., 2006, *AJ*, **131**, 1163

Stanek K. Z., 1996, *ApJ*, **460**, L37

Stanek K. Z., Garnavich P. M., 1998, *ApJ*, **503**, L131

Stasińska G., Tylenda R., Acker A., Stenholm B., 1992, *A&A*, **266**, 486

Stetson P. B., Bruntt H., Grundahl F., 2003, *PASP*, **115**, 413

Stutz A., Popowski P., Gould A., 1999, *ApJ*, **521**, 206

Sutherland W., et al., 2015, *A&A*, **575**, A25

Szymański M. K., Udalski A., Soszyński I., Kubiak M., Pietrzyński G., Poleski R., Wyrzykowski L., Ulaczyk K., 2011, *Acta. Astronom.*, **61**, 83

Thompson I. B., Kaluzny J., Rucinski S. M., Krzeminski W., Pych W., Dotter A., Burley G. S., 2010, *AJ*, **139**, 329

Tonry J. L., et al., 2012, *ApJ*, **750**, 99

Tylenda R., Acker A., Stenholm B., Koeppen J., 1992, *A&AS*, **95**, 337

Udalski A., 2003a, *Acta. Astronom.*, **53**, 291

Udalski A., 2003b, *ApJ*, **590**, 284

Udalski A., Szymanski M. K., Soszynski I., Poleski R., 2008, *Acta. Astronom.*, **58**, 69

Udalski A., Szymański M. K., Szymański G., 2015, *Acta. Astronom.*, **65**, 1

Wagner-Kaiser R., Sarajedini A., Dalcanton J. J., Williams B. F., Dolphin A., 2015, *MNRAS*, **451**, 724

Wang X., Wang L., Filippenko A. V., Zhang T., Zhao X., 2013, *Science*, **340**, 170

Wegg C., Gerhard O., 2013, *MNRAS*, **435**, 1874

Wegg C., Gerhard O., Portail M., 2015, *MNRAS*, **450**, 4050

Wolf C., 2014, *MNRAS*, **445**, 4252

Wozniak P. R., Stanek K. Z., 1996, *ApJ*, **464**, 233

Yee J. C., et al., 2015, *ApJ*, **810**, 155

Zasowski G., et al., 2009, *ApJ*, **707**, 510

Zasowski G., et al., 2015, *ApJ*, **798**, 35

Zoccali M., Hill V., Lecureur A., Barbuy B., Renzini A., Minniti D., Gómez A., Ortolani S., 2008, *A&A*, **486**, 177

Index	Colour 1	Colour 2
$(V - I)$	1.060	0.994
$(V - U)$	-2.217	-1.746
$(V - B)$	-1.115	-0.982
$(V - R)$	0.568	0.523
$(V - Z_{\text{Vista}})$	1.313	1.220
$(V - Y_{\text{Vista}})$	1.531	1.428
$(V - J_{\text{Vista}})$	1.893	1.773
$(V - H_{\text{Vista}})$	2.361	2.220
$(V - K_{s,\text{Vista}})$	2.518	2.355
$(V - J_{2\text{MASS}})$	1.852	1.734
$(V - H_{2\text{MASS}})$	2.378	2.236
$(V - K_{s,2\text{MASS}})$	2.525	2.361
$(V - u_{\text{SDSS}})$	-3.104	-2.620
$(V - g_{\text{SDSS}})$	-0.553	-0.476
$(V - r_{\text{SDSS}})$	0.327	0.288
$(V - i_{\text{SDSS}})$	0.600	0.543
$(V - z_{\text{SDSS}})$	0.759	0.683
$(V - F435W_{\text{ACS}})$	-1.161	-1.017
$(V - F475W_{\text{ACS}})$	-0.623	0.554
$(V - F555W_{\text{ACS}})$	-0.046	-0.040
$(V - F606W_{\text{ACS}})$	0.286	0.262
$(V - F814W_{\text{ACS}})$	1.079	1.015
$(V - F218W_{\text{WFC3}})$	-6.929	-6.576
$(V - F225M_{\text{WFC3}})$	-6.820	-6.118
$(V - F275W_{\text{WFC3}})$	-5.192	-4.300
$(V - F336W_{\text{WFC3}})$	-2.387	-1.845
$(V - F350lp_{\text{WFC3}})$	0.1430	0.127
$(V - F390m_{\text{WFC3}})$	-2.490	-2.087
$(V - F390W_{\text{WFC3}})$	-1.749	-1.458
$(V - F438W_{\text{WFC3}})$	-1.192	-1.036
$(V - F475W_{\text{WFC3}})$	-0.588	-0.522
$(V - F547M_{\text{WFC3}})$	0.004	0.007
$(V - F555W_{\text{WFC3}})$	-0.103	-0.092
$(V - F606W_{\text{WFC3}})$	0.271	0.248
$(V - F625W_{\text{WFC3}})$	0.491	0.451
$(V - F775W_{\text{WFC3}})$	0.993	0.935
$(V - F814W_{\text{WFC3}})$	1.070	1.006
$(V - F850LP_{\text{WFC3}})$	1.284	1.205
$(V - F098M_{\text{WFC3}})$	1.380	1.292
$(V - F110W_{\text{WFC3}})$	1.657	1.549
$(V - F125W_{\text{WFC3}})$	1.845	1.727
$(V - F140W_{\text{WFC3}})$	2.070	1.946
$(V - F160W_{\text{WFC3}})$	2.279	2.152
$(I - J_{\text{Vista}})$	0.833	0.779
$(J_{\text{Vista}} - K_{s,\text{Vista}})$	0.653	0.582

Table 1. Estimated mean photometric colours for the Galactic bulge red clump. In the second column (Colour 1), we assume a model atmosphere with $\log g = 2.2$, $[\text{Fe}/\text{H}] = 0.0$, $[\alpha/\text{Fe}] = 0.0$, and $T_{\text{eff}} = 4650\text{K}$, which yield the intrinsic red clump colours adopted in this work. In the third column (Colour 2), we assume $\log g = 2.2$, $[\text{Fe}/\text{H}] = -0.30$, $[\alpha/\text{Fe}] = +0.10$, and $T_{\text{eff}} = 4800\text{K}$. Colours are computed using the methodology of Casagrande & Vandenberg (2014), where the accuracy of synthetic colors is also discussed (in particular the shortcomings at blue and ultraviolet wavelengths). *UBVRI* and *WFC3* magnitudes are in the Vega system, *SDSS* magnitudes are in the *AB* system. Some of the colours are thus in a composite Vega-AB system.

	C89 $R_V = 3.1$ $A_V = 3$	C89 $R_V = 3.1$ $A_V = 6$	C89 $R_V = 2.5$ $A_V = 4$	F99 $R_V = 3.1$ $A_V = 4$	F99 $R_V = 2.5$ $A_V = 4$	FM07 $R_V = 3.001$ $A_V = 4$	FM07 (RRab) $R_V = 3.001$ $A_V = 4$
–							
A_V/A_{5500}	0.986	0.978	0.980	0.976	0.967	0.970	0.985
A_I/A_{5500}	0.588	0.583	0.542	0.557	0.524	0.524	0.527
A_J/A_{5500}	0.282	0.281	0.253	0.262	0.265	0.231	0.232
A_{K_s}/A_{5500}	0.119	0.119	0.107	0.117	0.120	0.087	0.087

Table 2. Extinction coefficients as a function of parameterization, R_V , A_V , and input stellar spectra for a few representative cases. The RR Lyrae spectrum assumes $T_{\text{eff}} = 6000$ K, $[\text{Fe}/\text{H}] = -1.0$, $[\alpha/\text{Fe}] = +0.40$, and $\log g = 2.0$.

RA	DEC	$E(V-I)$	$A_I/E(V-I)$	$E(I-J)/E(V-I)$	$E(J-K_s)/E(V-I)$
268.257367	-32.138720	1.566	1.243	0.775	0.308
268.435012	-32.119689	1.598	1.340	0.803	0.317
268.523834	-32.119689	1.430	1.248	0.799	0.309
268.301778	-32.119689	1.757	1.275	0.813	0.308
268.212956	-32.119689	1.522	1.272	0.772	0.308

Table 3. Representative sampling of the coordinates and extinction curve parameters for the 1,854 sightlines of this study deemed reliable, as per the criteria stated at the top of Section 5. Full table available as online material.

Index	Value	$R_{V,\text{C89}}$	$R_{V,\text{F99}}$
$A_{F625W}/(A_{F435W} - A_{F625W})$	1.25	1.97	2.46
$A_I/E(V-I)$	1.10	2.20	2.21
$E(I-J)/E(V-I)$	0.70	2.72	3.07
$E(J-K_s)/E(V-I)$	0.25	1.97	0.98
$E(J-K_s)/E(I-J)$	0.36	2.69	3.67

Table 4. The best-fit values of R_V as a function of extinction curve parameter for the parameterizations of [Cardelli et al. \(1989\)](#) and [Fitzpatrick \(1999\)](#) for the sightline investigated by [Revnivtsev et al. \(2010\)](#).